





Preparation and characterization of two new metal–organic coordination polymers with 3,3'-azodibenzoic acid under N-donor auxiliary chelating ligand intervention

Lei Zhang, Chu-Yue Jing, Ya-Qiang Zhong, Qing-Hua Meng & Kou-Lin Zhang

To cite this article: Lei Zhang, Chu-Yue Jing, Ya-Qiang Zhong, Qing-Hua Meng & Kou-Lin Zhang (2015) Preparation and characterization of two new metal–organic coordination polymers with 3,3'-azodibenzoic acid under N-donor auxiliary chelating ligand intervention, Journal of Coordination Chemistry, 68:22, 3954-3968, DOI: [10.1080/00958972.2015.1080362](https://doi.org/10.1080/00958972.2015.1080362)

To link to this article: <http://dx.doi.org/10.1080/00958972.2015.1080362>

 View supplementary material 

 Accepted author version posted online: 13 Aug 2015.
Published online: 07 Sep 2015.

 Submit your article to this journal 

 Article views: 93

 View related articles 

 View Crossmark data 

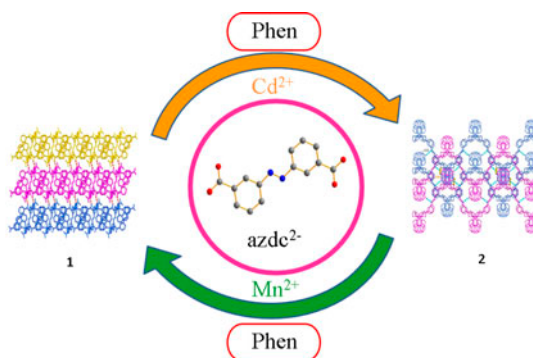
Preparation and characterization of two new metal–organic coordination polymers with 3,3'-azodibenzoic acid under *N*-donor auxiliary chelating ligand intervention

LEI ZHANG[†], CHU-YUE JING[†], YA-QIANG ZHONG[†], QING-HUA MENG[‡] and KOU-LIN ZHANG^{*†}

[†]Key Laboratory of Environmental Material and Environmental Engineering of Jiangsu Province, College of Chemistry and Chemical Engineering, Yangzhou University, Yangzhou, China

[‡]Jiangsu Key Laboratory of Green Synthesis for Functional Materials, Jiangsu Normal University, Xuzhou, China

(Received 30 November 2014; accepted 16 July 2015)



Reactions of 3,3'-azodibenzoic acid (H_2azdc) with Mn(II) and Cd(II) in the presence of 1,10-phenanthroline (phen) yield two new metal–organic coordination polymers, $\{[\text{Mn}(\text{azdc})(\text{phen})(\text{DMF})(\text{H}_2\text{O})]\}_n$ (**1**) and $\{[\text{Cd}(\text{azdc})(\text{phen})]\}_n$ (**2**), which display 1-D azdc-bridged coordination arrays with different topology. **1** was synthesized under ambient conditions and exhibits a *zigzag* chain structure, further extending into a 2-D supramolecular double layer through C–H $\cdots\pi$ and C–H \cdots O hydrogen bonds. Solvothermally **2** was obtained and shows a double-chain structure. Adjacent double chains are linked by C–H \cdots N hydrogen bonds to give a 2-D supramolecular wavy double layer. Distinct extended 3-D supramolecular network architectures are further constructed with weak secondary interactions, especially aromatic stacking and hydrogen bonding as supramolecular driving forces. The coordination modes of azdc^{2-} and crystalline architectures of the complexes depend on the central metal ions. The desolvation–resolvation behavior of **1** has been explored. Thermal stabilities of **1** and **2** have been studied. Solid-state fluorescence of **2** has been investigated.

Keywords: Coordination polymers; Synthesis; Crystal structures; Fluorescence; Desolvation–resolvation property

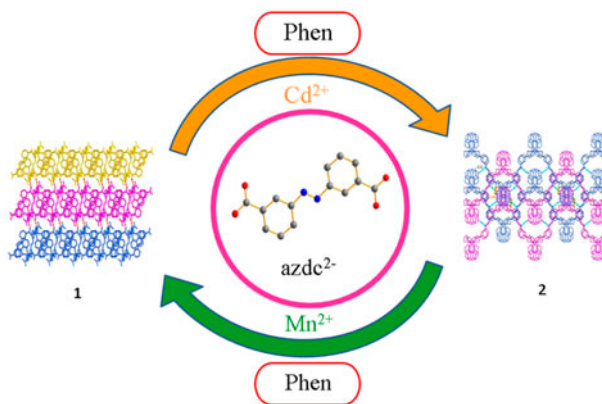
*Corresponding author. Email: klzhang@yzu.edu.cn

1. Introduction

One target of contemporary crystal engineering is the development of new metal–organic coordination polymers (MOCPs) with various functions and possible applications, such as molecular adsorption, magnetism, nonlinear optics, molecular sensing, heterogeneous catalysis, and photoactive materials, although the rational design and synthesis of MOCPs with desired structure and function remains a long-term challenge [1–11]. The construction of MOCPs depends on the combination of several factors, such as the coordination geometry of metal ions, the nature of organic ligands, the reaction temperature, the use of non-covalent interactions (hydrogen bonding, π – π interactions, or their combination in different ways), and sometimes, the reagent ratio [12–15]. Understanding, how these considerations affect metal coordination and influence crystal packing is at the forefront of controlling coordination arrays. Geometries of organic ligands play crucial roles in determining the polymeric structures [16].

Polycarboxylate aromatic ligands have been employed in the construction of multidimensional MOCPs. Carboxylates are attractive as metal-binding units in MOCPs because the negative charge enhances their ability to coordinate with metal nodes, contributing to stability of the resulting coordination polymers. A variety of coordination modes available to polycarboxylate-based ligands not only allow access to a wide variety of coordination polymers, but also make it difficult to predict coordination geometries and node connectivities [17–24]. Azo-based polycarboxylate systems, such as 3,3',5,5'-azobenzenetetracarboxylic acid (H_4abtc) and 3,3'-azodibenzoic acid (H_2azdc) representing one type of bridging aromatic polycarboxylate ligand, have been employed in generation of some MOCPs [25–30].

To better understand the coordination chemistry of azo-based polycarboxylate ligands and construction of the related MOCPs, recently, we have undertaken a systematic study of MOCPs with azo-based polybenzoate ligands. Herein, we describe our recent results of two new MOCPs with H_2azdc in the presence of auxiliary chelating phen, $\{[Mn(azdc)(phen)(DMF)(H_2O)]\}_n$ (**1**), and $[Cd(azdc)(phen)]_n$ (**2**) (scheme 1). **1** exhibits a zigzag chain structure, while **2** shows a double-chain structure. Both **1** and **2** further extend into a 2-D



Scheme 1. Simplified representation of the metal ion-dependent crystalline architectures and desolvation/resolution behaviors of **1** and **2**.

supramolecular double layer with the aid of hydrogen bonds. The desolvation–resolvation behavior of **1** has been investigated. Thermal stabilities of **1** and **2** have been studied. The solid-state fluorescent property of **2** has been explored.

2. Experimental

2.1. Materials and measurements

The 3,3'-azodibenzoic acid (H_2azdc) was prepared according to the literature method [31, 32]; other reagents were purchased commercially and used without purification. Elemental analyses (C, H, and N) were carried out on a 240-C Elemental analyzer. FT-IR spectra ($400\text{--}4000\text{ cm}^{-1}$) were recorded from KBr pellets in a Magna 750 FT-IR spectrophotometer. Powder X-ray diffraction (PXRD) data were collected at room temperature on a computer-controlled Bruker D8 Advanced XRD diffractometer equipped with Cu $K\alpha$ monochromator ($\lambda = 1.5418\text{ \AA}$) at a scanning rate of $0.024^\circ\text{ s}^{-1}$ from 5° to 50° . Solid-state fluorescence spectra were recorded using an F 4500 fluorescence spectrometer. Thermogravimetric analyses were taken on a NETZSCH STA 409 PG/PC instrument at a heating rate of 10°C min in N_2 .

2.2. Crystal structure determination

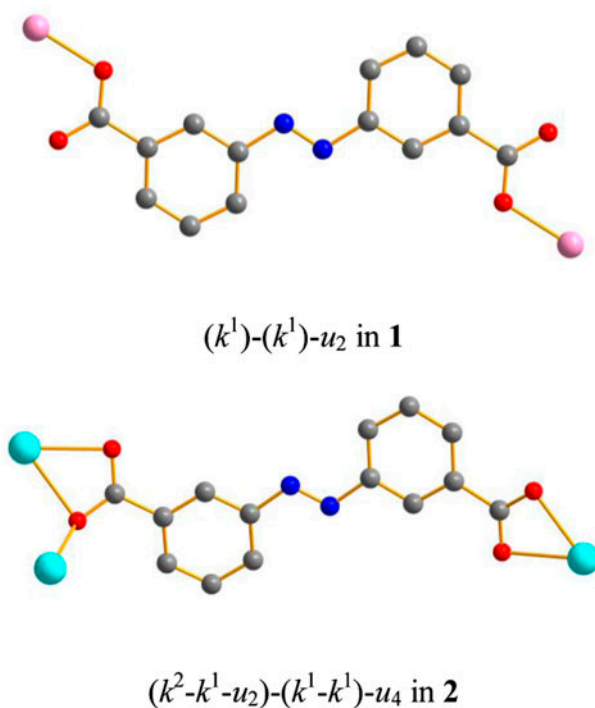
Crystallographic data were collected with a Siemens SMART CCD diffractometer using graphite-monochromated (Mo- $K\alpha$) radiation ($\lambda = 0.71073\text{ \AA}$), ψ and ω scans mode. The structures were solved by direct methods and refined by full-matrix least-squares on F^2 using SHELXL-97 [33]. Intensity data were corrected for Lorenz and polarization effects and a multiscan absorption correction was performed. All nonhydrogen atoms were refined anisotropically. The carbon-bound hydrogens of both complexes were added geometrically and allowed to ride on their respective parent. The oxygen-bound hydrogens of water were located in the difference Fourier map and then kept fixed. The contributions of these hydrogens were included in the structure factor calculations. Details of crystal data, collection, and refinement are listed in table 1.

2.3. Synthesis of the complexes

2.3.1. Synthesis of $\{[Mn(azdc)(phen)(DMF)(H_2O)]\}_n$ (1**).** A mixture of H_2azdc (0.027 g, 0.100 mmol) in DMF (5 mL) and NaOH (0.004 g, 0.100 mmol) (0.2 mL, 0.5 mol L^{-1}) was added to an aqueous solution of $MnCl_2\cdot 4H_2O$ (0.019 g, 0.1 mmol) in water (5 mL) while stirring. To this solution, phen (0.020 g, 0.100 mmol) in DMF (5 mL) was added. The filtrate was kept at ambient temperature for several days and pale yellow crystals were formed (yield: 48 mg, 80% based on H_2azdc). Anal. Calcd for $C_{29}H_{25}MnN_5O_6$: C, 58.59; H, 4.24; N, 11.78. Found: C, 58.49; H, 4.16; N, 11.65%. IR cm^{-1} (KBr): 3339(w), 3056(w), 1631(s), 1601(vs), 1556(vs), 1519(m), 1429(s), 1385(vs), 1212(w), 1094(m), 929(w), 846(s), 779(s), 719(s), 689(s), 667(w).

Table 1. Crystallographic and structure refinement data for **1** and **2**.

Complexes	1	2
Empirical formula	$C_{29}H_{25}MnN_5O_6$	$C_{26}H_{16}CdN_4O_4$
Formula weight	594.48	560.84
Wavelength (Å)	0.71073	0.71073
Crystal system	Triclinic	Monoclinic
Space group	<i>P</i> -1	<i>C</i> 2/ <i>c</i>
<i>a</i> (Å)	10.737(5)	27.000(3)
<i>b</i> (Å)	11.228(5)	10.6716(11)
<i>c</i> (Å)	13.315(6)	18.906(2)
α (°)	72.734(5)	90
β (°)	80.796(6)	121.6490(10)
γ (°)	63.896(6)	90
Volume (Å ³)	1375.7(11)	4637.3(9)
<i>Z</i>	2	8
Density (Mg m ⁻³)	1.435	1.607
Absorption coeff. (mm ⁻¹)	0.532	0.983
<i>F</i> (0 0 0)	614	2240
θ range for data collection (°)	1.60 to 25.00	1.77 to 27.52
Index ranges	$-12 \leq h \leq 12, -13 \leq k \leq 12, -14 \leq l \leq 15$	$-34 \leq h \leq 34, -13 \leq k \leq 13, -23 \leq l \leq 24$
Reflections collected	10,150	19,890
Unique	4816	5320
<i>R</i> _{int}	0.0852	0.0318
Completeness to θ	99.4%	99.5%
Max. and min. transmission	4816/3380	5320/0316
Goodness-of-fit on <i>F</i> ²	0.954	1.066
Final <i>R</i> indices [<i>I</i> > 2 σ (<i>I</i>)]	<i>R</i> ₁ = 0.0653, <i>wR</i> ₂ = 0.1399	<i>R</i> ₁ = 0.0304, <i>wR</i> ₂ = 0.0874
<i>R</i> indices (all data)	<i>R</i> ₁ = 0.1614, <i>wR</i> ₂ = 0.2043	<i>R</i> ₁ = 0.0467, <i>wR</i> ₂ = 0.0972
Largest diff. peak and hole (e Å ⁻³)	0.377 and -0.388	1.022 and -0.368



Scheme 2. Simplified representation of the coordination modes of azdc^{2-} in **1** and **2**.

2.3.2. Synthesis of $[\text{Cd}(\text{azdc})(\text{phen})]_n$ (2**).** A mixture containing $\text{Cd}(\text{NO}_3)_2 \cdot 4\text{H}_2\text{O}$ (0.016 g, 0.050 mmol), H_2azdc (0.027 g, 0.100 mmol), phen (0.020 g, 0.100 mmol), and the mixed water–DMF solvent (3 mL : 3 mL) was sealed in a Teflon reactor, which was heated at 120 °C for three days, and then cooled to room temperature at 5 °C h^{-1} . Dark red block crystals were collected in 56% yield (31 mg, based on H_2azdc). Anal. Calcd for $\text{C}_{26}\text{H}_{16}\text{CdN}_4\text{O}_4$: C, 55.68; H, 2.88; N, 9.99. Found: C, 55.79; H, 2.97; N, 9.89%. IR cm^{-1} (KBr): 3064(w), 1670(w), 1586(vs), 1556(vs), 1429(s), 1391(vs), 1220(w), 1145(w), 854(s), 817(s), 779(s), 727(s), 667(m).

The phase purities of **1** and **2** were further verified by the PXRD data of the bulk samples which are consistent with the corresponding simulated ones from single-crystal X-ray diffraction data (figure 5 for **1** and figure S1 for **2**).

3. Results and discussion

3.1. Synthesis of the complexes

The assembly between Mn(II) and Cd(II) with H_2azdc in the presence of phen leads to **1** and **2**. It should be noted that **2** can only be synthesized solvothermally, while **1** can only be synthesized using typical solution method at ambient temperature. NaOH was used to neutralize the acid. The molar ratio of $\text{H}_2\text{asba}:\text{NaOH}$ is important for the growth of single

crystals. The molar ratios of $\text{H}_2\text{asba}:\text{NaOH}$ (1:1 for **1** and 1:0 for **2**) were used during the synthesis. During the synthesis of **1** and **2**, if *N,N*-dimethylacetamide (DMA) was used as the mixed cosolvent, the same products as **1** and **2** were obtained, indicating that DMF and DMA have almost no influence on the construction of **1** and **2**. All the carboxylate groups in **1** and **2** are deprotonated as verified by IR spectra (see below) and the results of crystallographic analysis (vide post). The work presented here also indicates that the central metal ions, Cd(II)/Mn(II), affect the crystalline architectures and consequently tuning the functional properties of the resulting MOCs.

3.2. Crystal structure descriptions

3.2.1. Structural description of $\{[\text{Mn}(\text{azdc})(\text{phen})(\text{DMF})(\text{H}_2\text{O})]\}_n$ (1**).** Complex **1** crystallizes in the triclinic system with space group *P*-1 and has a *zigzag* chain structure. Each Mn(II) is six coordinate by two nitrogens from phen and two oxygens from two carboxylate groups of two different azdc^{2-} ligands, one oxygen from coordinated water, and one oxygen

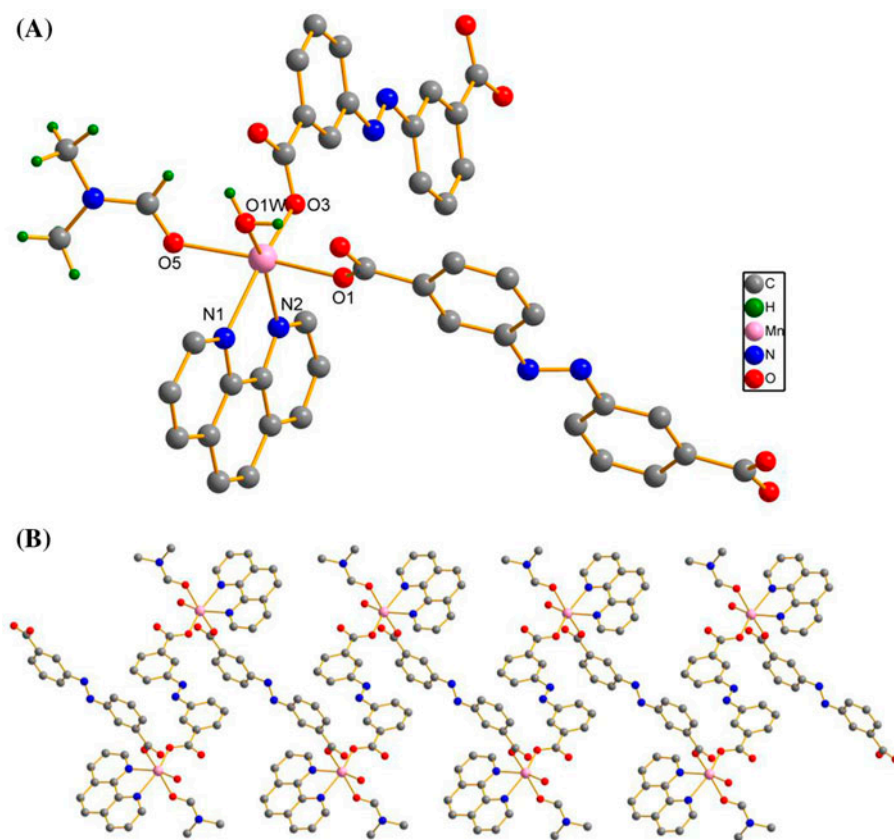


Figure 1. (A) The coordination environment of Mn(II) in **1**. (B) *Zigzag* chain. (C) 2-D supramolecular double layer formed through C-H...O and C-H... π interactions. (D) 3-D supramolecular network directed by interlayer hydrogen bonds.

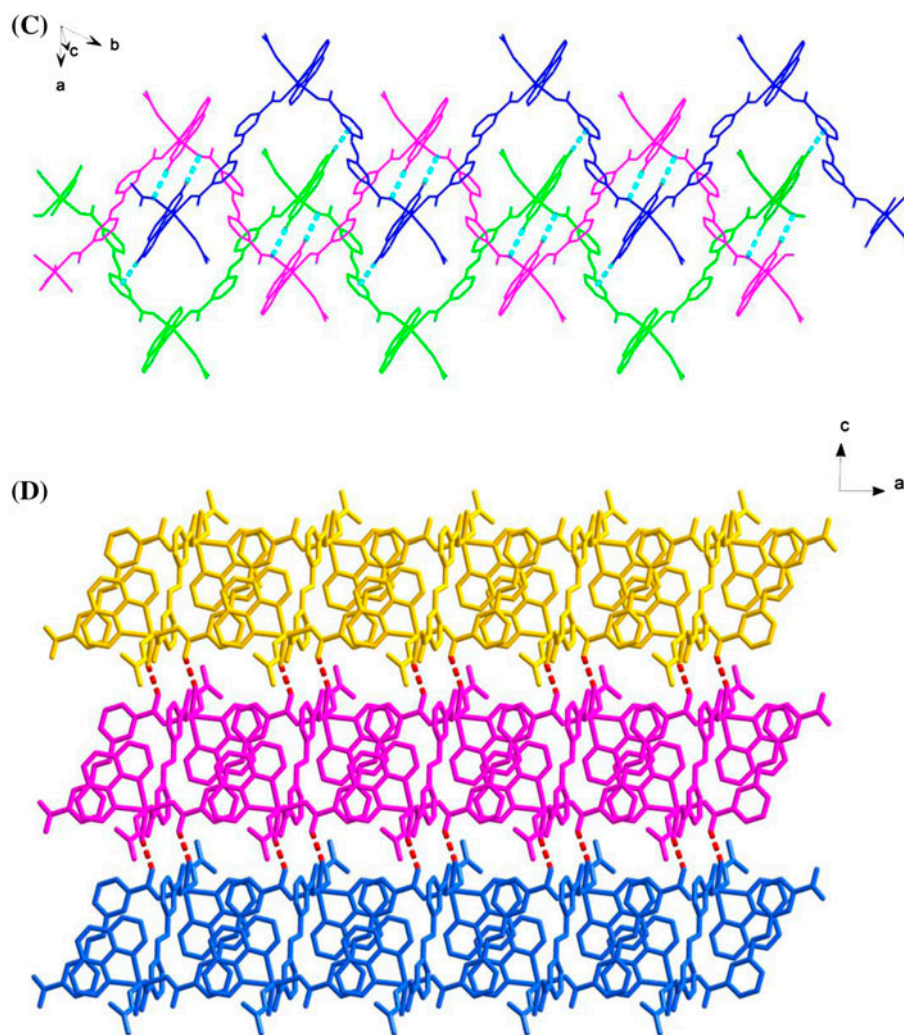


Figure 1. (Continued).

from coordinated DMF, adopting a distorted octahedral coordination geometry [figure 1(A), table 2]. Each azdc^{2-} bridges two Mn(II) centers in bis-monodentate (k^1)-(k^1)- u_2 bridging to form a zigzag chain [scheme 2, figure 1(B)] with the intrachain Mn...Mn distances of 15.162 and 15.371 Å, respectively, whereas the closest interchain Mn...Mn distance is 10.737 Å. The chain structure of **1** is quite different from that of reported Mn(II) complex based on 5,5'-dithiobis(2-nitrobenzoate) and phen, which consists of a paddle wheel-shaped SBU [17c]. The chains run along the *b*-axis and connect with each other through the strong C17-H17... π interaction [the distance between the H17 and the centroid of the nearest aromatic ring (C1-C6) in azdc^{2-} : 2.563 Å] and the C11-H11...O1 hydrogen bonds (3.514 Å) between the aromatic carbon (C11)-bonded hydrogen H11 and coordinated oxygen atom O1 of carboxylate group in the nearest chain. If these C17-H17... π interactions and

Table 2. Selected bond lengths and angles for **1** and **2**.

Complex 1			
Mn(1)–O(3)	2.141(4)	Mn(1)–N(2)	2.299(5)
Mn(1)–O(1 W)	2.174(5)	Mn(1)–N(1)	2.301(5)
Mn(1)–O(1)	2.189(4)	Mn(1)–O(5)	2.245(5)
O(1 W)–Mn(1)–O(1)	84.11(18)	O(3)–Mn(1)–O(5)	95.73(17)
O(1 W)–Mn(1)–O(5)	86.17(19)	O(1)–Mn(1)–O(5)	167.95(16)
O(3)–Mn(1)–N(2)	85.88(18)	O(1 W)–Mn(1)–N(2)	156.54(19)
O(1)–Mn(1)–N(2)	87.93(16)	O(5)–Mn(1)–N(2)	98.32(18)
O(3)–Mn(1)–N(1)	156.06(18)	O(1 W)–Mn(1)–N(1)	86.67(19)
O(1)–Mn(1)–N(1)	92.33(17)	O(5)–Mn(1)–N(1)	80.00(18)
O(3)–Mn(1)–O(1 W)	116.73(18)	O(3)–Mn(1)–O(1 W)	116.73(18)
N(2)–Mn(1)–N(1)	71.62(19)		
Complex 2			
Cd(1)–O(3)#2	2.316(2)	Cd(1)–O(2)	2.410(2)
Cd(1)–O(1)	2.335(3)	Cd(1)–N(1)	2.416(2)
Cd(1)–N(2)	2.358(2)	Cd(1)–O(4)#3	2.424(2)
Cd(1)–O(3)#3	2.498(3)		
O(3)#2–Cd(1)–O(1)	100.04(10)	O(3)#2–Cd(1)–N(2)	140.31(8)
O(1)–Cd(1)–N(2)	102.69(8)	O(3)#2–Cd(1)–O(2)	90.21(9)
O(1)–Cd(1)–O(2)	55.05(8)	N(2)–Cd(1)–O(2)	129.47(9)
O(3)#2–Cd(1)–N(1)	79.54(8)	O(1)–Cd(1)–N(1)	86.18(8)
N(2)–Cd(1)–N(1)	70.06(8)	O(2)–Cd(1)–N(1)	137.63(8)
O(3)#2–Cd(1)–O(4)#3	107.97(9)	O(1)–Cd(1)–O(4)#3	125.00(9)
N(2)–Cd(1)–O(4)#3	84.65(8)	O(2)–Cd(1)–O(4)#3	78.13(8)
N(1)–Cd(1)–O(4)#3	144.15(8)	O(3)#2–Cd(1)–O(3)#3	78.56(9)
O(1)–Cd(1)–O(3)#3	176.59(7)	N(2)–Cd(1)–O(3)#3	80.19(8)
O(2)–Cd(1)–O(3)#3	121.70(7)	N(1)–Cd(1)–O(3)#3	96.58(7)
O(4)#3–Cd(1)–O(3)#3	53.09(7)		

Symmetry transformations: #2 $-x + 3/2, -y - 1/2, -z + 1$; #3 $x + 1/2, -y - 1/2, z + 1/2$ for **2**.

C11–H11 \cdots O1 hydrogen bonds are considered, then the zigzag chains were extended into a 2-D supramolecular double layer [figure 1(C)]. It should be noted that such C17–H17 $\cdots\pi$ interaction also exists in the Mn(II) complex based on the 4-(benzimidazol-1-ylmethyl)benzoate ligand [16d].

Further investigation on the crystal packing indicates that 2-D supramolecular double layers are arranged in a parallel fashion along [0 1 0] direction and assembled into a 3-D supramolecular network by the interlayer O1W–H1WA \cdots O4 [3.805(4) Å] hydrogen bonds, in which O4 is the uncoordinated oxygen in the carboxylate group O3C29O4 of the adjacent double layer [figure 1(D)].

3.2.2. Structural description of {[Cd(azdc)(phen)]_n (2)}. Complex **2** contains one unique Cd(II), one azdc²⁻ ligand, and one phen in each asymmetric unit. The Cd(II) shows a single-capped trigonal prism coordination geometry [CdN₂O₅] completed by five carboxylate oxygens from three azdc²⁻ ligands and two nitrogens from phen [figure 2(A)]. The bond lengths of Cd–O_{carboxylate} and Cd–N_{phen} are within normal ranges (table 2), also in agreement with those in the other reported Cd(II) complex [16c]. The carboxylate group O3C7O4 from azdc²⁻ exhibits chelating/bridging conformation, resulting in the formation of centrosymmetrical carboxylate-bridged dinuclear secondary building unit (SBU) [Cd₂(COO)₂(phen)₂]. The other carboxylate group O1C8O2 shows chelating coordination.

So, azdc^{2-} has $(k^2-k^1-u_2)-(k^1-k^1)-u_4$ coordination (scheme 2). The $\text{Cd1}\cdots\text{Cd1\#2}$ (#2: $-x+3/2, -y-1/2, -z+1$) separation in each SBU is 3.725 Å. There are strong offset $\pi\cdots\pi$ stacking interactions between the symmetric pyridyl rings (C15–C18N1) of phen [the centroid–centroid distance: 3.587 Å] within the SBU. The SBUs were double linked by azdc^{2-} , resulting in formation of the zigzag double chain [figure 2(B)]. The chains are parallel with each other. Adjacent chains are linked by $\text{C16-H16}\cdots\text{N3}_{\text{azo}}$ [2.6282(2) Å] hydrogen bonds to give a 2-D supramolecular wavy double layer [figure 2(C)].

$\text{C22-H22}\cdots\text{O1}$ [2.421(2) Å] hydrogen bonds exist between the 2-D supramolecular double layers (table 3). The phen ligands are alternately located at both sides of this 2-D pattern in a slanted fashion. The phen segments in each chain are stretched outward to produce the space sites for offset aromatic $\pi\cdots\pi$ stacking with those from two neighboring chains in the adjacent layers evidenced by the distance between the centroids of C20–24N2 and C18–C21C25C26): 3.6283(3) Å, which is quite different from the structure of **1**. So, in this manner, these 2-D supramolecular layers, organized in a sequence of A(–A) centrosymmetry operation), are extended into a 3-D supramolecular network [figure 2(D)].

3.3. FT-IR spectra and thermogravimetric analyses

The FT-IR spectral data show features attributable to the carboxylate stretching vibrations of both **1** and **2** (figure S2). The absence of bands from 1680 to 1760 cm^{-1} indicates complete

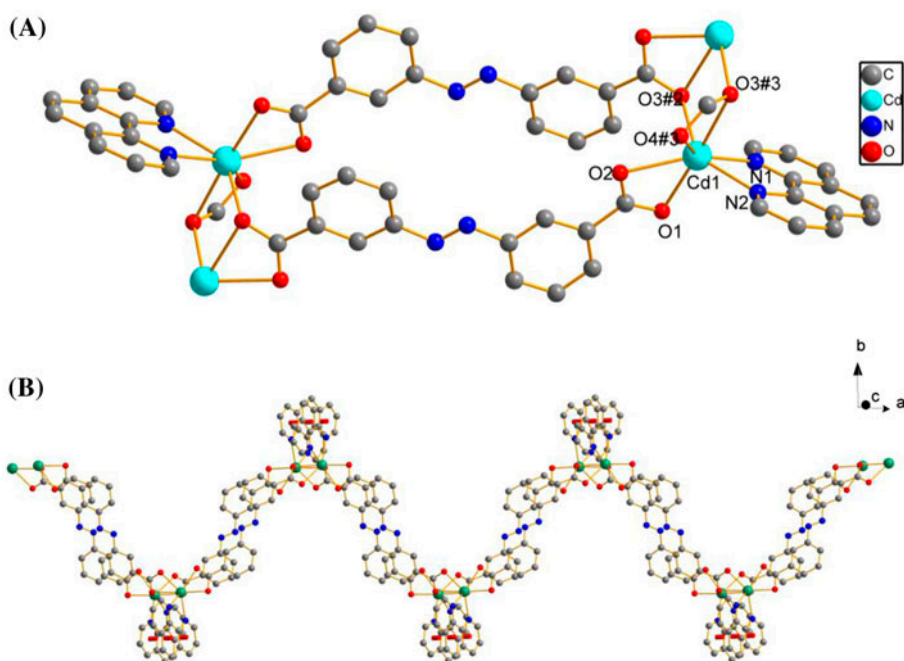


Figure 2. (A) View of the coordination geometry of the Cd(II) and centrosymmetrical dinuclear SBU unit in **2**. Symmetry transformations: #2 $-x+3/2, -y-1/2, -z+1$; #3 $x+1/2, -y-1/2, z+1/2$, (B) Zigzag double chain, (C) 2-D supramolecular double layer formed through $\text{C16-H16}\cdots\text{N3}$ [2.6282(2) Å] hydrogen bonds and (D) 3-D supramolecular network showing the $\text{C24-H24}\cdots\text{O1}$ [2.421(2) Å] hydrogen bonds and interlayer strong offset $\pi\cdots\pi$ stacking interactions connecting the adjacent 2-D supramolecular layers.

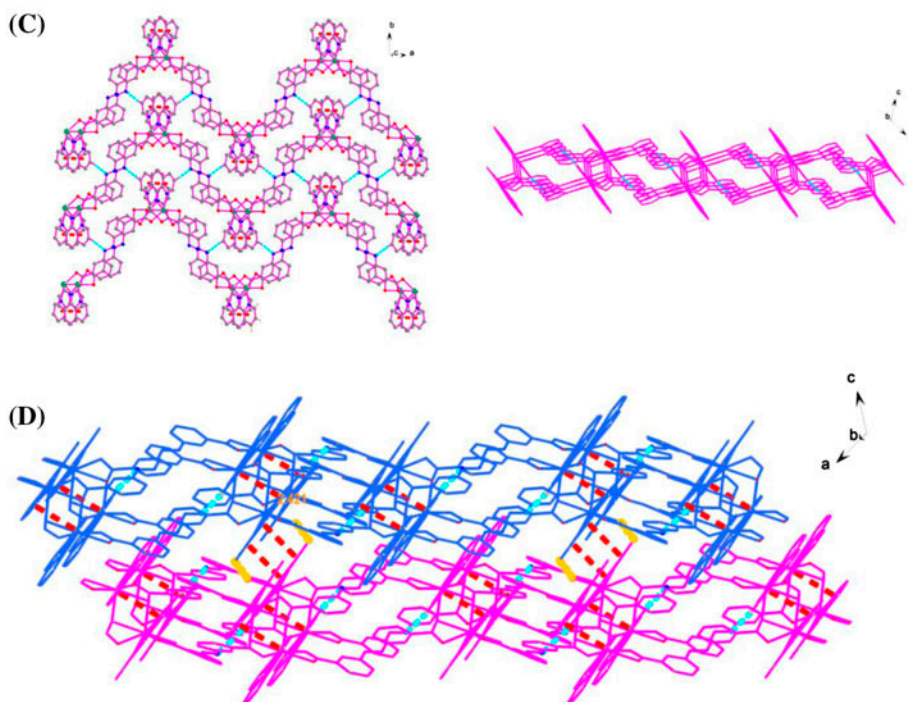


Figure 2. (Continued).

deprotonation of H_2azdc in these complexes. In the FT-IR spectrum of **1**, the broad band centered around 3339 cm^{-1} corresponds to the $-\text{OH}$ stretching vibrations of water and the band at 1631 cm^{-1} may be attributed to the stretching vibration of the amide group $-\text{CON}-$ in DMF. The characteristic bands of the carboxylate groups are $1556\text{--}1601\text{ cm}^{-1}$ for the asymmetric stretch and $1391\text{--}1429\text{ cm}^{-1}$ for the symmetric stretch [34].

To study the thermal stability of the materials, the thermogravimetric analysis (TG) was performed on all samples under a nitrogen atmosphere in flowing N_2 with a heating rate of $10\text{ }^\circ\text{C min}^{-1}$ (figure 3). TGA of **1** suggests that **1** exhibits a weight loss of 12.12% from 104 to $160\text{ }^\circ\text{C}$, corresponding to loss of both coordinated water and DMF molecules (Calcd 12.78%). The second weight loss beginning at $347\text{ }^\circ\text{C}$ corresponds to decomposition of the framework.

Table 3. The details of the hydrogen bonds for **1** and **2**.

D-H...A	d(D-H)	d(H...A)	d(D...A)	$\angle\text{DHA}$	Symmetry of A
Complex 1					
O1 W-H1 WA...O4	0.86(5)	1.86(5)	2.714(6)	174(7)	$2-x, 1-y, -z$
O1W-H1WB...O2	0.86(11)	1.75(10)	2.583(8)	162(9)	
C10-H10...O3	0.9300	2.5400	3.118(8)	121.00	
C20-H20...O4	0.9300	2.4600	3.266(9)	145.00	$2-x, 1-y, -z$
C11-H11...O1	0.9300	2.603(1)	3.514(9)	166.33(7)	
Complex 2					
C22-H22...O1	0.9300	2.4200	3.147(4)	135.00	$2-x, 1-y, 1-z$

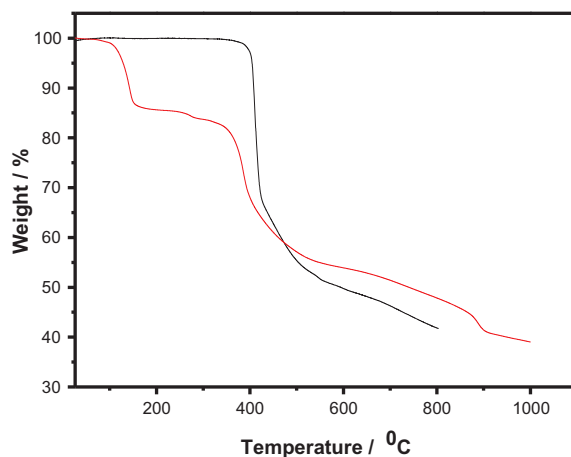


Figure 3. TGA curves of **1** (red) and **2** (black) (see <http://dx.doi.org/10.1080/00958972.2015.1080362> for color version).

No weight loss is observed below 370 °C in the TG curve of **2**, which further confirms the absence of lattice water in the phase. Complex **2** decomposes at 370 °C, revealing that **2** has high framework stability.

3.4. UV–vis spectra

The solid-state diffuse reflectance UV–vis spectra of free acid H_2azdc and **1** have similar shapes (figure 4). The sharp absorption maximum at 310 nm in **1** is attributed to the $n \rightarrow \pi^*$ transition of $\text{C}=\text{O}$ in azdc^{2-} . The red shifts of the maximum absorption and weak strengths compared with that in free H_2azdc (297 nm) may result from the coordination effect of azdc^{2-} . In addition, we observed an additional weak shoulder at 400–540 nm for **1**, which may originate from the d–d spin-forbidden transition of the d^5 (Mn^{2+}) ion [35, 36].

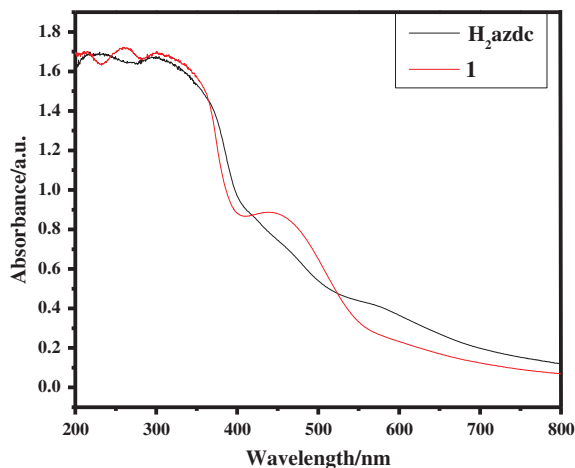


Figure 4. The solid-state diffuse UV–vis reflectance spectra of **1** (red) and H_2azdc (black) (see <http://dx.doi.org/10.1080/00958972.2015.1080362> for color version).

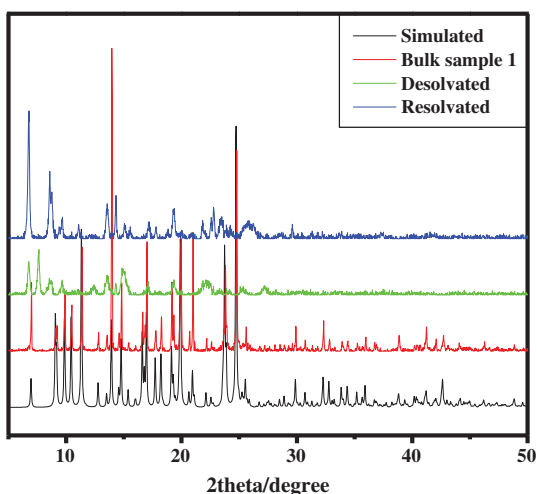


Figure 5. The PXRD patterns of **1**.

3.5. Desolvation–resolution of **1**

Thermogravimetric analyses (TGA) show clearly that both the coordinated water and DMF in **1** could be excluded upon heating. To study the desolvation–resolution property of **1**, the *in situ* variable temperature PXRD was performed on **1** from 30 to 160 °C for **1** in air (figure 5). The PXRD patterns clearly show that **1** undergoes irreversible desolvation–resolution behavior; upon exposure of the desolvated material in the mixed DMF and water solvent for about one week, the desolvated phase resolves, resulting in a new phase which is different from the original crystal structure. The desolvated phase of **1** still retains its integrity after both the DMF and water molecules are lost, but the structure of the

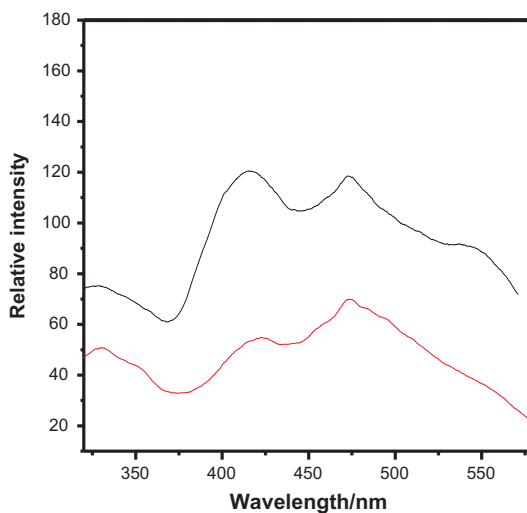


Figure 6. Solid-state fluorescence emissions recorded at room temperature for H₂azdc (red) and **2** (black) ($\lambda_{\text{ex}} = 300$ nm) (see <http://dx.doi.org/10.1080/00958972.2015.1080362> for color version).

desolvated material is changed, as supported by the *in situ* variable temperature PXRD pattern. This observation clearly indicates that during desolvation–resolvation in **1** the framework exhibits a phase transition.

3.6. Fluorescent property

The fluorescent properties of **2** together with the free acid H₂azdc were studied in the solid state at room temperature. To compare the relative fluorescent intensities of **2** and H₂azdc, we determined both emission spectra with the same excitation wavelength. The emission spectra of **2** and H₂azdc have been measured under the same condition (slit width = 5 nm). Excitation of **2** and free H₂azdc at 300 nm leads to the generation of similar blue fluorescent emissions with the maximum emission centered at 473 nm and a shoulder at 415 nm (figure 6). These observations suggest that coordination of azdc²⁻ with Cd(II) in the presence of phen as auxiliary ligand has almost no influence on the emission mechanism of the compound [37]. Therefore, the fluorescence of **2** may be ligand-based emission, ascribed to the intraligand $\pi \rightarrow \pi^*$ or $n \rightarrow \pi^*$ transitions of azdc²⁻ [38, 39]. The relatively stronger fluorescence intensity of **2** compared with that of H₂azdc may be attributed to ligation of azdc²⁻ to the d¹⁰ Cd(II) center enhancing the rigidity of the ligand and reducing the loss of energy through a radiationless pathway [40, 41].

4. Conclusion

The present study further shows that azdc²⁻ can act as convenient building blocks for construction of MOCPs. In this way, Mn(II)/Cd(II) MOCPs based on H₂azdc were generated with their architectures dependent on the central metal nodes. **1** exhibits a *zigzag* chain structure, while **2** exhibits a double-chain structure. These two CPs further extend into a 3-D supramolecular network through hydrogen bonding and strong offset $\pi \cdot \cdot \pi$ stacking interactions. **1** shows irreversible desolvation–resolvation behavior. **2** exhibits blue fluorescent bands in the solid state. This work gives us impetus to further investigate the coordination chemistry of azdc²⁻ and fabrication of the related MOCPs.

Supplementary material

Crystallographic data have been deposited with the Cambridge Crystallographic Data Center with Nos. 1016752 (**1**) and 1016751 (**2**). Copies of the data can be obtained free of charge via the Internet at <http://www.ccdc.cam.ac.uk/conts/retrieving.html>.

Acknowledgments

We gratefully acknowledge the Natural Science Foundation of Jiangsu Province (BK2012680), the Priority Academic Program Development of Jiangsu Higher Education Institutions (PAPD), the Analysis and Test Center of Yangzhou University, and the Key Laboratory of Environmental Material and Environmental Engineering of Jiangsu Province.

Disclosure statement

No potential conflict of interest was reported by the authors.

Supplemental data

The supplemental data for this paper is available online at <http://dx.doi.org/10.1080/00958972.2015.1080362>.

References

- [1] J. An, S.J. Geib, N.L. Rosi. *J. Am. Chem. Soc.*, **132**, 38 (2010).
- [2] B.H. Ye, M.L. Tong, X.M. Chen. *Coord. Chem. Rev.*, **249**, 545 (2005).
- [3] R. Matsuda, R. Kitaura, S. Kitagawa, Y. Kubota, R.V. Belosludov, T.C. Kobayashi, H. Sakamoto, T. Chiba, M. Takata, Y. Kawazoe, Y. Mita. *Nature*, **436**, 238 (2005).
- [4] P.L. Llewellyn, P. Horcajada, G. Maurin, T. Devic, N. Rosenbach, S. Bourrelly, C. Serre, D. Vincent, S. Loera-Serna, Y. Filinchuk, G. Férey. *J. Am. Chem. Soc.*, **131**, 13002 (2009).
- [5] J.M. Lehn. *Supramolecular Chemistry: Concepts and Perspectives*, VCH, New York (1995).
- [6] A.G. Wong-Foy, A.J. Matzger, O.M. Yaghi. *J. Am. Chem. Soc.*, **128**, 3494 (2006).
- [7] J. Lee, O.K. Farha, J. Roberts, K.A. Scheidt, S.T. Nguyen, J.T. Hupp. *Chem. Soc. Rev.*, **38**, 1450 (2009).
- [8] W.J. Rieter, K.M. Pott, K.M.L. Taylor, W. Lin. *J. Am. Chem. Soc.*, **130**, 11584 (2008).
- [9] Y.Y. Niu, H.G. Zheng, H.W. Hou, X.Q. Xin. *Coord. Chem. Rev.*, **248**, 169 (2004).
- [10] X.H. Bu, W. Chen, S.L. Lu, R.H. Zhang, D.Z. Liao, W.M. Bu, M. Shionoya, F. Brisse, J. Ribas. *Angew. Chem. Int. Ed.*, **40**, 3201 (2001).
- [11] X.H. Zhou, Y.H. Peng, X.D. Du, C.F. Wang, J.L. Zuo, X.Z. You. *Cryst. Growth Des.*, **9**, 1028 (2009).
- [12] J. Yang, J.F. Ma, Y.Y. Liu, J.C. Ma, S.R. Batten. *Inorg. Chem.*, **46**, 6542 (2007).
- [13] S.R. Fan, L.G. Zhu. *Inorg. Chem.*, **46**, 6785 (2007).
- [14] X.P. Li, J.Y. Zhang, M. Pan, S.R. Zheng, Y. Liu, C.Y. Su. *Inorg. Chem.*, **46**, 4617 (2007).
- [15] D.F. Sava, V.C. Kravtsov, J. Eckert, J.F. Eubank, F. Nouar, M. Eddaoudi. *J. Am. Chem. Soc.*, **131**, 10394 (2009).
- [16] (a) F. Dai, H. He, D. Gao, F. Ye, X. Qiu, D. Sun. *CrystEngComm*, **11**, 2516 (2009); (b) X.L. Zhao, W.Y. Sun. *CrystEngComm*, **16**, 3247 (2014); (c) J.J. Yang, J.J. Zhang, X.Y. Yu, Y.H. Luo, H. Zhang. *J. Coord. Chem.*, **66**, 689 (2013); (d) H.W. Kuai, X.C. Cheng, X.H. Zhu. *J. Coord. Chem.*, **66**, 28 (2013).
- [17] (a) C.D. Wu, C.Z. Lu, W.B. Yang, S.F. Lu, H.H. Zhuang, J.S. Huang. *Eur. J. Inorg. Chem.*, **4**, 797 (2002); (b) Y.N. Zhang, Z. Dong, X. Hai, L. Cui, Y.Y. Wang. *J. Coord. Chem.*, **66**, 1676 (2013); (c) W.P. Wu, X.R. Wu, L. Lu, J. Wang. *J. Coord. Chem.*, **68**, 130 (2015).
- [18] Y. Go, X. Wang, E.V. Anokhina, A.J. Jacobson. *Inorg. Chem.*, **43**, 5360 (2004).
- [19] Y. Li, N. Hao, Y. Lu, E. Wang, Z. Kang, C. Hu. *Inorg. Chem.*, **42**, 3119 (2003).
- [20] K.L. Zhang, Y. Chang, C.T. Hou, G.-W. Diao, R. Wu, S.W. Ng. *CrystEngComm*, **12**, 1194 (2010).
- [21] K.L. Zhang, C.T. Hou, J.J. Song, Y. Deng, L. Li, S.W. Ng, G.W. Diao. *CrystEngComm*, **14**, 590 (2012).
- [22] Z.Z. Lin, F.L. Jiang, D.Q. Yuan, L. Chen, Y.F. Zhou, M.C. Hong. *Eur. J. Inorg. Chem.*, **10**, 1927 (2005).
- [23] Z.Z. Lin, F.L. Jiang, L. Chen, D.-Q. Yuan, Y.F. Zhou, M.C. Hong. *Eur. J. Inorg. Chem.*, **1**, 77 (2005).
- [24] C.J. Kepert, T.J. Prior, M.J. Rosseinsky. *J. Am. Chem. Soc.*, **122**, 5158 (2000).
- [25] Z.F. Chen, R.G. Xiong, B.F. Abrahams, X.Z. You, C.M. Che. *J. Chem. Soc., Dalton Trans.*, 2453 (2001).
- [26] T.M. Reineke, M. Eddaoudi, D. Moler, M. O'Keeffe, O.M. Yaghi. *J. Am. Chem. Soc.*, **122**, 4843 (2000).
- [27] Y.F. Han, X.Y. Li, L.Q. Li, C.L. Ma, Z. Shen, Y. Song, X.Z. You. *Inorg. Chem.*, **49**, 10781 (2010).
- [28] J.S. Guo, G. Xu, G.C. Guo, J.S. Huang. *Cryst. Growth Des.*, **13**, 2642 (2013).
- [29] L.L. Liu, C.X. Yu, J. Sun, P.P. Meng, F.J. Ma, J.M. Du, L.F. Ma. *Dalton Trans.*, **43**, 2915 (2014).
- [30] Y.L. Liu, J.F. Eubank, A.J. Cairns, J. Eckert, V.C. Kravtsov, R. Luebke, M. Eddaoudi. *Angew. Chem., Int. Ed.*, **46**, 3278 (2007).
- [31] F. Rakotondrany, M.A. Whitehead, A.M. Lebus, H.F. Sleiman. *Chem. Eur. J.*, **9**, 4771 (2003).
- [32] V. Kannappan, P. Sathyamoorthi, D.R. Singh. *J. Polym. Mater.*, **19**, 65 (2002).
- [33] G.M. Sheldrick, *SHELXL 97, Programs for Crystal Structure Analysis* (Release 97-2), University of Göttingen, Germany (1997).
- [34] K. Nakamoto. *Infrared and Raman Spectra of Inorganic and Coordination Compounds*, Wiley, New York (1986).
- [35] J. Zhao, X.L. Wang, X. Shi, Q.H. Yang, C. Li. *Inorg. Chem.*, **50**, 3198 (2011).
- [36] C.F. Naumann, H. Sigel. *J. Am. Chem. Soc.*, **96**, 2750 (1974).

- [37] S.T. Wang, Y. Hou, E.B. Wang, Y.G. Li, L. Xu, J. Peng, S.X. Liu, C.W. Hu. *New J. Chem.*, **27**, 1144 (2003).
- [38] Y.J. Cui, Y.F. Yue, G.D. Qian, B.L. Chen. *Chem. Rev.*, **10**, 1126 (2012).
- [39] S.J.A. Pope, B.J. Coe, S. Faulkner, E.V. Bichenkova, X. Yu, K.T. Douglas. *J. Am. Chem. Soc.*, **126**, 9490 (2004).
- [40] S.L. Zheng, J.M. Yang, X.L. Yu, X.M. Chen, W.T. Wong. *Inorg. Chem.*, **43**, 830 (2004).
- [41] S.L. Zheng, M.L. Tong, S.D. Tan, Y. Wang, J.X. Shi, Y.X. Tong, H.K. Lee, X.M. Chen. *Organometallics*, **20**, 5319 (2001).